

Vector Single-Source Surface Integral Equation for TE Scattering From Cylindrical Multilayered Objects

Zekun Zhu, *Graduate Student Member, IEEE*, Xiaochao Zhou, *Graduate Student Member, IEEE*, Shunchuan Yang, *Member, IEEE*, Zhizhang (David) Chen, *Fellow, IEEE*

Abstract—A single-source surface integral equation (SS-SIE) for transverse electric (TE) scattering from cylindrical multilayered objects is proposed in this paper. By incorporating the differential surface admittance operator (DSAO) and recursively applying the surface equivalence theorem from innermost to outermost boundaries, an equivalent model with only electric current density on the outermost boundary can be obtained. In addition, an integration approach is proposed, where the small argument expansion of the Hankel function is used to evaluate the singular and nearly singular integrals. Compared with other SIEs, such as the Poggio-Miller-Chang-Harrington-Wu-Tsai (PMCHWT) formulation, the computational expenditure is reduced for multilayered structures because only a single source is needed on the outermost boundary. As shown in the numerical results, the proposed method generates only 19% of unknowns, uses 26% of memory, and requires 29% of the CPU time of the PMCHWT formulation.

Index Terms—Multilayers, method of moments, single-source formulation, surface equivalence theorem, singularity cancellation, TE polarization

I. INTRODUCTION

THE two-dimensional transverse electric (TE) electromagnetic waves find many practical engineering applications, such as microwave imaging [1], remote sensing [2], and electromagnetic absorbing materials [3]. The method of moments (MoM) is widely used to solve the TE electromagnetic problems. One of the most commonly used surface-integral-equations (SIEs) is the Poggio-Miller-Chang-Harrington-Wu-Tsai (PMCHWT) formulation [4, Ch. 4, pp. 160-188]. In it, dual sources of both electric and magnetic current densities are considered and solved on each interface of different media. Several techniques, like the combined tangential formulation (CTF) [5], the Müller formulation [6], and the multiple-trace PMCHWT (MT-PMCHWT) [7], are proposed to improve SIE

matrix conditioning and computational efficiency. However, when two or more regions are encountered, a large system of linear equations often results.

Several methods are proposed to decrease the size or dimension of the system, like single-source formulations without either magnetic currents or electric currents. In [8]-[10], a single-source surface-volume-surface (SS-SVS) formulation is proposed to solve the TE scattering problems of penetrable objects. In [11], a generalized impedance boundary condition (GIBC) is used to model interconnects without magnetic current density. In [12], the differential surface admittance operator (DSAO) without a magnetic current is proposed to model two-dimensional rectangular interconnects. It is extended into other practical applications [13]-[21]. Other forms of single-source methods are also proposed to model penetrable objects [22]-[25].

Besides the above single-source formulations, equivalence principle algorithms (EPAs) [26] [27] with both electric and magnetic current densities are proposed to solve three-dimensional scattering problems. In [28], the EPA combined with a connection scheme is proposed to model periodic perfectly electric conductors (PECs) embedded in planar multilayer media for TM scattering. Through the recursive application of the boundary conditions to the interfaces between two different planar media, multi-layer scattering problems can be efficiently solved. In the EPAs, both electric and magnetic current densities are required on a closed surface as a result of Love's equivalence theorem [29, Ch.12, pp. 653-658]. However, when objects are fully embedded in multilayers, the methods mentioned above may suffer from efficiency problems due to the rapid increase of unknowns at each interface.

Other efforts are made to improve the accuracy and robustness for nearly singular and singular integrals in the three-dimensional space [30]-[37]. Green's function in the three-dimensional space is $e^{-jkR}/(4\pi R)$, and in two-dimensional, the Green's function is the Hankel function $H_0^{(2)}(\cdot)$, which is the infinite summation of polynomials. They all have the singularity. A singularity cancellation approach is proposed to solve the $\log(R)$ singularity in [38], where the entire-domain basis functions are used in the two-dimensional TM analysis. In [39], the analytical approach for potential integrals of the logarithmic function $\log(R)$ is introduced based on the small argument expansion of $H_0^{(2)}(\cdot)$. In [40], a mechanical quadrature approach is proposed to handle the singularity

Manuscript received xxx; revised xxx.

This work was supported in part by the National Natural Science Foundation of China through Grant 61801010, Grant 62071125, Grant 61427803, and Grant 61631002, in part by Fundamental Research Funds for the Central Universities. (*Corresponding author: Shunchuan Yang*)

Z. Zhu, and X. Zhou are with the School of Electronic and Information Engineering, Beihang University, Beijing, 100083, China. (e-mail: zekun-zhu@buaa.edu.cn, zhouchao@buaa.edu.cn)

S. Yang is with the Research Institute for Frontier Science and the School of Electronic and Information Engineering, Beihang University, Beijing, 100083, China. (e-mail: scyang@buaa.edu.cn)

Z. Chen is with College of Physics and Information Engineering, Fuzhou University and on leave from the Department of Electrical and Computer Engineering, Dalhousie University, Halifax, NS, Canada B3J 2X4. (e-mail: z.chen@dal.ca)

for two-dimensional circular PECs. Only the self-interactions are considered to be singular, and the analytical integration is used to calculate the singular integration, as described in [8] [13] [41, Ch.3, pp. 43-44] [42] [43, Ch.6, pp. 125-137]. However, when the small argument expansion is used, the self-interaction segments may not fully satisfy the small argument condition, or near segments may also needed to be considered. As a result, those approaches may not get accurate enough results.

To mitigate the problems described above, a new vector SS-SIE is proposed to solve the TE scattering problems of cylindrical multilayered objects (see Fig. 1(a)). The surface equivalence theorem [29, Ch.12, pp. 653-658] is recursively applied from the innermost to outermost boundaries, and original objects are replaced by the background medium, as shown in Fig. 1(b). Furthermore, by incorporating the DSAO [12], only the equivalent electric current density is needed on the *outermost* boundary, and the computational expenditure is reduced. In addition, an integration approach, which combines numerical and analytical integration, is proposed to calculate singular and nearly singular integrals.

It should be noted that the proposed SS-SIE formulation is different from those presented in [44], in which the Green's function is constructed by recursively uniting fictitious cells with the block inversion of the full-matrix [11]. The proposed formulation directly uses the surface equivalence theorem on each interface and calculates the equivalent current densities. Compared with the conventional methods [11] [44], the proposed formulation has a physical interpretation rather than purely mathematical manipulations.

The proposed SS-SIE formulation is also different from that presented in [45]. In [45], a recursive single-source equation is proposed for scattering by composite objects, in which a pair of exclusive operators are defined to calculate electromagnetic fields. The surface equivalent current densities at interior boundaries are assumed to be related to those on the outermost boundary. In the final system, the current densities on the inner boundaries are to be solved.

The contributions in this paper are twofold:

- 1) A new vector SS-SIE formulation is proposed to solve the TE scattering by penetrable or PEC objects embedded in multilayers. For a complex, multilayered structure, the unknowns on all the boundaries do not have to be solved simultaneously, but are coupled into the outer boundary. It reduces the dimension of the matrix, and thus the computational expenditures. It is built on our previous work of [46] [47].
- 2) An integration approach is proposed to handle various types of singular and nearly singular integrals in the proposed SS-SIE formulation. By combining numerical integration and analytical integration, the matrix elements can be accurately and efficiently calculated. The number of Gaussian points can be reduced to less than ten to reach the machine level.

This paper is organized as follows. In Section II, the proposed SS-SIE formulation is described. In Section III, by combining the surface current density and the electric field integral equation (EFIE) on the outermost boundary, the

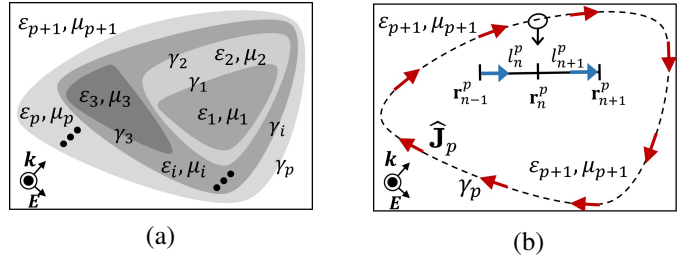


Fig. 1. (a) The TE scattering on objects embedded in multilayers. (b) The equivalent model with the electric current density enforced on the outermost boundary γ_i .

proposed SS-SIE formulation to solve the exterior scattering problem is presented. In Section IV, the proposed integration approach is described. In Section V, the accuracy of the proposed integration approach and the performance of the proposed SS-SIE are investigated with several numerical examples. At last, we draw some conclusions in Section VI.

II. METHODOLOGY

A. The Configurations and Preliminaries

The TE scattering on cylindrical multilayered objects with arbitrary cross-sections is considered as shown in Fig. 1(a). The penetrable object with constant material parameters ϵ_i and μ_i is enclosed by its boundary γ_i . Assume that there are p layers, and the background medium is with the constant material parameters ϵ_{p+1} and μ_{p+1} . Each boundary is discretized with N_1, N_2, \dots, N_p line segments. Based on the surface equivalence theorem [29, Ch. 12, pp. 653-658], the scattering fields can be regarded as generated by surface electric and magnetic current densities on the boundary enclosing the objects. Since the fields outside the objects are of interested, fields inside objects can be *arbitrary* in the equivalent problem. Therefore, the single electric current density $\hat{\mathbf{J}}_p$ enforced on the outermost boundary can be obtained through carefully selecting the fields inside objects, as shown in Fig. 1(b).

Before we move to detailed formulation derivation, some notations used are introduced. A bold character denotes a vector, and if it has a subscript i , the vector is defined on the boundary γ_i . A hollow character denotes a matrix, and it has the subscript (i, j) and a superscript (k) . It means that the source and observation points are on γ_i and γ_j , respectively. k means that the surface equivalence theorem is applied for the k th time. A quantity with a wide hat $\hat{}$ denotes that it is for the equivalent configuration. An inner product is defined as

$$\langle \mathbf{f}, \mathbf{g} \rangle = \int \mathbf{f} \cdot \mathbf{g} \, dr. \quad (1)$$

B. The SS-SIE for A Penetrable Object Embedded in the Background Medium

A single penetrable object is first considered. We reported the preliminary idea in [48]. Detailed formulations are presented in this subsection.

According to the Stratton-Chu formulation [49, Ch. 1, pp. 38-48], the electric field \mathbf{E} inside γ_i can be expressed as

$$T\bar{\mathbf{t}}_i(\mathbf{E}) = \bar{\mathbf{t}}_i(\mathcal{L}_i[\mathbf{n}'_i \times \mathbf{H}_i]) + \bar{\mathbf{t}}_i(\mathcal{K}_i[\mathbf{n}'_i \times \mathbf{E}_i]), \quad (2)$$

where

$$\bar{\mathbf{t}}_i(\mathbf{A}_i) = \mathbf{n}_i \times \mathbf{n}_i \times \mathbf{A}_i(\mathbf{r}), \quad (3)$$

$$\mathcal{L}_i(\mathbf{A}_i) = -j\omega\mu(1 + \frac{1}{k_i^2} \nabla \nabla \cdot) \oint_{\gamma_i} G_i(\mathbf{r}, \mathbf{r}') \mathbf{A}_i(\mathbf{r}') d\mathbf{r}', \quad (4)$$

$$\mathcal{K}_i(\mathbf{A}_i) = \nabla \times \int_{\gamma_i} \mathbf{A}_i(\mathbf{r}') G_i(\mathbf{r}, \mathbf{r}') d\mathbf{r}'. \quad (5)$$

\mathcal{L}_i and \mathcal{K}_i are both linear operators, and \mathcal{K}_i is the Cauchy principal value without including the residual term. \mathbf{n}_i denotes a unit normal vector pointing to the interior region of γ_i , the Green's function is $G_i(\mathbf{r}, \mathbf{r}') = -(j/4) H_0^{(2)}(k_i |\mathbf{r} - \mathbf{r}'|)$ inside the penetrable object, and $H_0^{(2)}(\cdot)$ is the zeroth order Hankel function of the second kind. k_i represents the wave number inside γ_i . $T = 1/2$ when \mathbf{r} and \mathbf{r}' are located on the same boundary, otherwise, $T = 1$.

The dual vector basis function $\mathbf{f}_n^i(\mathbf{r}')$ [43, Ch. 2, pp. 92] and $\mathbf{n}'_i \times \mathbf{f}_n^i(\mathbf{r}')$ are used to expand $\mathbf{n}'_i \times \mathbf{H}_i$ and $\mathbf{n}'_i \times \mathbf{E}_i$, which are defined as

$$\mathbf{f}_n^i(\mathbf{r}') = \begin{cases} \frac{\mathbf{r}' - \mathbf{r}_{n-1}^i}{l_n^i}, & \mathbf{r}' \in [\mathbf{r}_{n-1}^i, \mathbf{r}_n^i] \\ \frac{\mathbf{r}_{n+1}^i - \mathbf{r}'}{l_{n+1}^i}, & \mathbf{r}' \in [\mathbf{r}_n^i, \mathbf{r}_{n+1}^i] \end{cases}, \quad (6)$$

where $\mathbf{f}_n^i(\mathbf{r}')$ is the n th basis function on γ_i , l_n^i and l_{n+1}^i are the length of the n th and $(n+1)$ th segments, and \mathbf{r}_{n-1}^i , \mathbf{r}_n^i , \mathbf{r}_{n+1}^i are the endpoints of the n th and $(n+1)$ th segments as shown in Fig. 1(b), respectively. $\mathbf{f}_n^i(\mathbf{r}')$ mimics the RWG basis function in three-dimensional space, and the total charge density for each adjacent segment pair is zero [43, Ch. 8, pp. 259]. Therefore, $\mathbf{n}'_i \times \mathbf{E}_i$ and $\mathbf{n}'_i \times \mathbf{H}_i$ can be expanded as

$$\mathbf{n}'_i \times \mathbf{E}_i = \sum e_n^i \mathbf{n}'_i \times \mathbf{f}_n^i(\mathbf{r}'), \quad (7)$$

$$\mathbf{n}'_i \times \mathbf{H}_i = \sum h_n^i \mathbf{f}_n^i(\mathbf{r}'). \quad (8)$$

It should be noted that $\mathbf{n}'_i \times \mathbf{E}_i$ is expanded through the dual vector basis function $\mathbf{n}'_i \times \mathbf{f}_n^i(\mathbf{r}')$, so that the residual term on the left-hand side (LHS) of (2) can be well tested by $\mathbf{f}_m^i(\mathbf{r})$ [50].

When we fix the observation points on γ_i , and $\mathbf{f}_m^i(\mathbf{r})$ is used to test (2), the following matrix equation can be obtained

$$\frac{1}{2} \mathbb{U}_{(i,i)} \mathbf{E}_i = \mathbb{L}_{(i,i)}^{(1)} \mathbf{H}_i + \mathbb{K}_{(i,i)}^{(1)} \mathbf{E}_i. \quad (9)$$

The entities of matrices $\mathbb{U}_{(i,i)}$, $\mathbb{L}_{(i,i)}^{(1)}$ and $\mathbb{K}_{(i,i)}^{(1)}$ are computed as follows

$$\begin{aligned} [\mathbb{U}_{(i,i)}]_{mn} &= -\langle \mathbf{f}_m, \bar{\mathbf{t}}(\mathbf{f}_n) \rangle, \\ [\mathbb{L}_{(i,j)}^{(k)}]_{mn} &= -\langle \mathbf{f}_m, \bar{\mathbf{t}}(\mathcal{L}_i(\mathbf{f}_n)) \rangle, \\ [\mathbb{K}_{(i,j)}^{(k)}]_{mn} &= -\langle \mathbf{f}_m, \bar{\mathbf{t}}(\mathcal{K}_i[\mathbf{n}'_i \times \mathbf{f}_n]) \rangle, \end{aligned} \quad (10)$$

where $\mathbb{U}_{(i,i)}$, $\mathbb{L}_{(i,j)}^{(k)}$ and $\mathbb{K}_{(i,j)}^{(k)}$ are square matrices with the dimension of $N_i \times N_i$, $N_j \times N_i$, and $N_j \times N_i$. $\mathbb{U}_{(i,i)}$ is defined without the superscript since it only depends on the boundary

segments. \mathbf{E}_i and \mathbf{H}_i are two column vectors including the expansion coefficients defined as follows

$$\mathbf{E}_i = [e_1^i, e_2^i, \dots, e_n^i, \dots, e_{N_1}^i]^T, \quad (11)$$

$$\mathbf{H}_i = [h_1^i, h_2^i, \dots, h_n^i, \dots, h_{N_1}^i]^T, \quad (12)$$

and e_n^i, h_n^i denote the n th coefficients of the basis functions defined on γ_i . By moving the second term on the right-hand side (RHS) of (9) to its LHS and inverting the square coefficient matrix, we get

$$\mathbf{H}_i = \underbrace{[\mathbb{L}_{(i,i)}^{(1)}]^{-1} [\frac{1}{2} \mathbb{U}_{(i,i)} - \mathbb{K}_{(i,i)}^{(1)}]}_{\mathbb{Y}_i} \mathbf{E}_i, \quad (13)$$

where \mathbb{Y}_i is the surface admittance operator (SAO) [12] for the original problem.

After the surface equivalence theorem is applied, the penetrable object is replaced by its surrounding medium, and surface equivalent current density is introduced to ensure fields in the exterior region unchanged. With a similar procedure above, we obtain

$$\hat{\mathbf{H}}_i = \underbrace{[\hat{\mathbb{L}}_{(i,i)}^{(1)}]^{-1} [\frac{1}{2} \mathbb{U}_{(i,i)} - \hat{\mathbb{K}}_{(i,i)}^{(1)}]}_{\hat{\mathbb{Y}}_i} \mathbf{E}_i, \quad (14)$$

where $\hat{\mathbb{Y}}_i$ is the SAO for the equivalent problem, and k_{i+1} should be used in (14), since ε_i and μ_i have been replaced by ε_{i+1} and μ_{i+1} . $\hat{\mathbf{H}}_i$, $\hat{\mathbb{L}}_{(i,i)}^{(1)}$, and $\hat{\mathbb{K}}_{(i,i)}^{(1)}$ with wide hat are calculated in the equivalent configuration. It should be noted that there is no hat for \mathbf{E}_i , since we make the tangential electric fields on γ_i unchanged in the equivalent configuration.

Therefore, based on the tangential magnetic boundary condition, the surface equivalent electric current density can be expressed as

$$\hat{\mathbf{J}}_i = \hat{\mathbf{H}}_i - \mathbf{H}_i = \underbrace{(\hat{\mathbb{Y}}_i - \mathbb{Y}_i)}_{\mathbb{Y}_{\gamma_i}} \mathbf{E}_i, \quad (15)$$

where $\hat{\mathbf{J}}_i$ is the expansion coefficients stored in a column vector when the equivalent current density on γ_i is expanded by $\mathbf{f}_n^i(\mathbf{r}')$, and \mathbb{Y}_{γ_i} is the DSAO on γ_i .

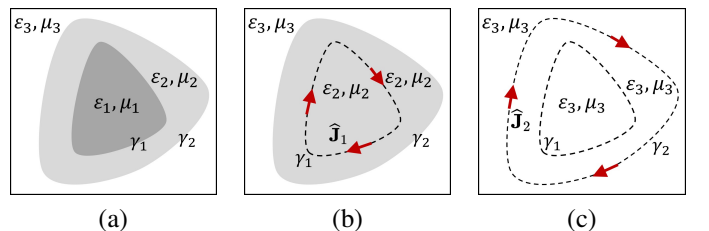


Fig. 2. (a) Two-layered penetrable object is embedded in the background region. (b) The equivalent current density $\hat{\mathbf{J}}_1$ is introduced on γ_1 after ε_1, μ_1 is replaced by ε_2, μ_2 . (c) The equivalent current density $\hat{\mathbf{J}}_1$ is transferred to γ_2 , and the medium inside γ_2 is replaced by ε_3, μ_3 .

C. The SS-SIE for A Two-layered Object Embedded in the Background Medium

Let's consider a two-layered object surrounding by γ_3 , as shown in Fig. 2(a). Our goal is to derive a surface equivalent

electric current density $\widehat{\mathbf{J}}_2$ enforced on the outermost boundary γ_2 through recursively applying the surface equivalence theorem from γ_1 to γ_2 . The proposed SS-SIE formulation is also applicable to the scenario when the PEC objects are embedded inside γ_i . The derivations are elaborated in the following paragraphs.

1) *A Dielectric Object in the Inner Region:* By applying the formulation in Section III-C, the inner penetrable object inside γ_1 is replaced by its surrounding medium, and a surface equivalent current density $\widehat{\mathbf{J}}_1$ is obtained on γ_1 , as shown in Fig. 2(b).

For a homogeneous object with an electric current density, the electric fields on γ_2 can be expressed through the Stratton-Chu formulation [49] as

$$T\bar{\mathbf{t}}_i(\mathbf{E}) = \bar{\mathbf{t}}_i(\mathcal{L}_2[\mathbf{n}'_2 \times \mathbf{H}_2(\mathbf{r}')] + \bar{\mathbf{t}}_i(\mathcal{K}_2[\mathbf{n}'_2 \times \mathbf{E}_2(\mathbf{r}')] + \bar{\mathbf{t}}_i[\mathcal{L}_1(\widehat{\mathbf{J}}_1)]. \quad (16)$$

Then, we fix the observation points on γ_1 to calculate \mathbf{E}_1 for (16). The following matrix equation is obtained

$$\mathbb{U}_{(1,1)}\mathbf{E}_1 = \mathbb{L}_{(2,1)}^{(2)}\mathbf{H}_2 + \mathbb{K}_{(2,1)}^{(2)}\mathbf{E}_2 + \mathbb{L}_{(1,1)}^{(2)}\widehat{\mathbf{J}}_1, \quad (17)$$

where $\widehat{\mathbf{J}}_1$, \mathbf{E}_2 , \mathbf{H}_2 denote the coefficient column vectors of the current density on γ_1 and tangential electric and magnetic fields on γ_2 , respectively.

By substituting (15) into (17), moving the last term on the RHS of (17) to its LSH and then inverting the square coefficient matrix, we obtain

$$\mathbf{E}_1 = \underbrace{\left[\mathbb{U}_{(1,1)} - \mathbb{L}_{(1,1)}^{(2)} \mathbb{Y}_{\gamma_1} \right]^{-1}}_{\mathbb{C}_{\gamma_1}} \left[\mathbb{L}_{(2,1)}^{(2)}\mathbf{H}_2 + \mathbb{K}_{(2,1)}^{(2)}\mathbf{E}_2 \right]. \quad (18)$$

Similarly, when the observation points are fixed on γ_2 to test (16), we have

$$\frac{1}{2}\mathbb{U}_{(2,2)}\mathbf{E}_2 = \mathbb{L}_{(2,2)}^{(2)}\mathbf{H}_2 + \mathbb{K}_{(2,2)}^{(2)}\mathbf{E}_2 + \mathbb{L}_{(1,2)}^{(2)}\widehat{\mathbf{J}}_1. \quad (19)$$

By substituting (15) and (18) into (19) and rearranging each term, the relationship between the tangential electric and magnetic field on γ_2 can be expressed as

$$\mathbf{H}_2 = \mathbb{Y}_2\mathbf{E}_2, \quad (20)$$

where

$$\mathbb{Y}_2 = \underbrace{\left[\mathbb{L}_{(2,2)}^{(2)} + \mathbb{L}_{(1,2)}^{(2)} \mathbb{Y}_{\gamma_1} \mathbb{C}_{\gamma_1} \mathbb{L}_{(2,1)}^{(2)} \right]^{-1}}_{\mathbb{V}_{\gamma_2}} \left[\frac{1}{2}\mathbb{U}_{(2,2)} - \mathbb{K}_{(2,2)}^{(2)} - \mathbb{L}_{(1,2)}^{(2)} \mathbb{Y}_{\gamma_1} \mathbb{C}_{\gamma_1} \mathbb{K}_{(2,1)}^{(2)} \right]. \quad (21)$$

\mathbb{C}_{γ_1} in (18) and \mathbb{V}_{γ_2} in (21) are both the matrices that require to be inverted. We will study the conditioning in Section V.

2) *A PEC Object in the Innermost Region:* When the innermost embedded object is PEC, a physical current \mathbf{J}_1 rather than the equivalent current $\widehat{\mathbf{J}}_1$ exists and the tangential

electric fields vanish on γ_1 . Therefore, \mathbf{E}_1 is equal to zero on the LHS of (17), and we get

$$\mathbf{0} = \mathbb{L}_{(2,1)}^{(2)}\mathbf{H}_2 + \mathbb{K}_{(2,1)}^{(2)}\mathbf{E}_2 + \mathbb{L}_{(1,1)}^{(2)}\mathbf{J}_1. \quad (22)$$

By inverting the square matrix $\mathbb{L}_{(1,1)}^{(2)}$, we get

$$\mathbf{J}_1 = -\left[\mathbb{L}_{(1,1)}^{(2)} \right]^{-1} \left[\mathbb{L}_{(2,1)}^{(2)}\mathbf{H}_2 + \mathbb{K}_{(2,1)}^{(2)}\mathbf{E}_2 \right]. \quad (23)$$

Then, after substituting (23) into (19) and rearranging each term, we have

$$\mathbf{H}_2 = \mathbb{Y}_{\text{PEC}}\mathbf{E}_2, \quad (24)$$

where

$$\mathbb{Y}_{\text{PEC}} = \left[\mathbb{L}_{(2,2)}^{(2)} - \mathbb{L}_{(1,2)}^{(2)} \left[\mathbb{L}_{(1,1)}^{(2)} \right]^{-1} \mathbb{L}_{(2,1)}^{(2)} \right]^{-1} \left[\frac{1}{2}\mathbb{U}_{(2,2)} - \mathbb{K}_{(2,2)}^{(2)} - \mathbb{L}_{(1,2)}^{(2)} \left[\mathbb{L}_{(1,1)}^{(2)} \right]^{-1} \mathbb{K}_{(2,1)}^{(2)} \right]. \quad (25)$$

3) *The Equivalent Problem:* After the surface equivalence theorem is applied on γ_2 , the object is replaced by the background medium, and there is no current source inside γ_2 , as shown in Fig. 2(c). When k_3 is used for (10), we obtain

$$\widehat{\mathbf{H}}_2 = \underbrace{\left[\widehat{\mathbb{L}}_{(2,2)}^{(2)} \right]^{-1} \left[\frac{1}{2}\mathbb{U}_{(2,2)} - \widehat{\mathbb{K}}_{(2,2)}^{(2)} \right]}_{\widehat{\mathbb{V}}_2} \mathbf{E}_2. \quad (26)$$

The surface electric current density \mathbf{J}_2 on γ_2 can be expressed as

$$\mathbf{J}_2 = \widehat{\mathbf{H}}_2 - \mathbf{H}_2 = \underbrace{\left(\widehat{\mathbb{V}}_2 - \mathbb{Y}_{2/\text{PEC}} \right)}_{\mathbb{Y}_{\gamma_2}} \mathbf{E}_2, \quad (27)$$

where \mathbb{Y}_{γ_2} is the DSAO on γ_2 . Note that $\mathbb{Y}_{2/\text{PEC}}$ is (21) for the penetrable object or (25) for the PEC object.

Compared with the macromodeling approach proposed in [18] for antenna array modeling, which is applicable for the PEC object embedded in the background medium, this paper's approach is applicable for more general scenarios including both penetrable and PEC objects. In addition, as shown in the later subsection, the proposed SS-SIE formulation is still suitable for objects embedded in multilayers.

D. Extension of the Proposed Formulation for Objects Embedded in Multilayers

To generalize the proposed SS-SIE formulation for cylindrical multilayered objects, the surface equivalence theorem is recursively applied from γ_1 to γ_p through the procedure in Section II-D. Eventually, the equivalent current density $\widehat{\mathbf{J}}_p$ on γ_p can be expressed as

$$\widehat{\mathbf{J}}_p = \mathbb{Y}_{\gamma_p}\mathbf{E}_p, \quad (28)$$

where \mathbb{Y}_{γ_p} is defined as the DASO on γ_p , which relates the tangential electric field to the surface equivalent current density on γ_p . Detailed recursive formulations are similar to those in [47].

III. SCATTERING MODELING OF THE PROPOSED SS-SIE

Once the equivalent current density $\hat{\mathbf{J}}_p$ on γ_p is derived, the scattering problem shown in Fig. 1 can be solved by using the EFIE. The total electric field \mathbf{E} in the exterior region is the superposition of the incident field \mathbf{E}^{inc} and the scattered field, which is expressed as

$$\mathbf{E}(\mathbf{r}) = -j\omega\mu \int_{\gamma_p} \left(1 + \frac{1}{k_{p+1}^2} \nabla' \nabla' \right) \hat{\mathbf{J}}_p(\mathbf{r}') G_{p+1}(\mathbf{r}, \mathbf{r}') d\mathbf{r}' + \mathbf{E}^{inc}(\mathbf{r}), \quad (29)$$

where \mathbf{r}' is on the outermost boundary γ_p , and the wavenumber k_{p+1} in the background medium should be used. Through fixing the observation points on γ_p , we have

$$\mathbb{U}_{(p,p)} \mathbf{E}_p = \mathbb{L}_{(p,p)}^{(p)} \mathbb{Y}_{\gamma_p} \mathbf{E}_p + \mathbf{E}^{in}. \quad (30)$$

The entries of \mathbf{E}^{in} are expressed as

$$[\mathbf{E}^{in}]_m = -\langle \mathbf{f}_m^p, \bar{\mathbf{t}}_p(\mathbf{E}^{inc}) \rangle. \quad (31)$$

Therefore, the scattering problem can be solved, and \mathbf{E}_p on γ_p is expressed as

$$\mathbf{E}_p = \left[\mathbb{U}_{(p,p)} - \mathbb{L}_{(p,p)}^{(p)} \mathbb{Y}_{\gamma_p} \right]^{-1} \mathbf{E}^{in}. \quad (32)$$

IV. CALCULATION OF SINGULAR AND NEARLY SINGULAR INTEGRALS IN THE PROPOSED SS-SIE FORMULATION

In this Section, a general configuration is presented in Fig. 3 to demonstrate the geometrical relationship between the observation point and the source segment. The notations in Fig. 3 are the same as those of [39]. \mathbf{r}'_1 and \mathbf{r}'_2 are the endpoints of the source segment $[\mathbf{r}'_1, \mathbf{r}'_2]$, \mathbf{r} is the observation point, \mathbf{r}' is the source point located on $[\mathbf{r}'_1, \mathbf{r}'_2]$, \mathbf{p} is the projection point from \mathbf{r} to $(\mathbf{r}'_1 - \mathbf{r}'_2)$, τ' is the unit vector of $(\mathbf{r}'_1 - \mathbf{r}'_2)$, and \mathbf{n}' is the unit normal vector.

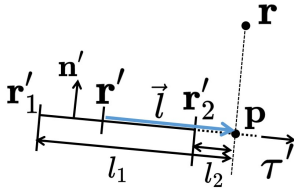


Fig. 3. A general scenario to demonstrate the geometrical relationship between the observation point and the source segment. $l_1 = (\mathbf{r}'_1 - \mathbf{r}) \cdot \tau'$, $l_2 = (\mathbf{r}'_2 - \mathbf{r}) \cdot \tau'$, $\vec{l} = \tau' \cdot [(\mathbf{r}' - \mathbf{r}) \cdot \tau']$.

For the integration in (4) and (5), the small variable expansion [39] is used to analytically calculate the results. According to [39], when $|k(\mathbf{r} - \mathbf{r}')| < \delta$ (δ is the threshold value to control the accuracy), we use the first-order approximation of

$H_0^{(2)}(\cdot)$ and $H_1^{(2)}(\cdot)$ to evaluate them, and the Green's function and its gradient can be expressed as

$$G(|k(\mathbf{r} - \mathbf{r}')|) \approx -\frac{j}{4} \left[1 - j \frac{2}{\pi} \ln \left(\frac{\gamma |k(\mathbf{r} - \mathbf{r}')|}{2} \right) \right], \quad (33)$$

$$\nabla' G(|k(\mathbf{r} - \mathbf{r}')|) \approx -\frac{j}{4} \left(\frac{k^2}{2} + \frac{2j}{\pi |\mathbf{r} - \mathbf{r}'|^2} \right) (\mathbf{r} - \mathbf{r}'), \quad (34)$$

where γ is the natural exponential of the Euler constant, and 16 effective digits are used in all simulations. Euler constant is approximated as 0.5772156649. The accuracy of the approximation is given in Fig. 4 for various δ . The reference results are obtained through the Matlab command “besselj(order, δ)” and “bessely(order, δ)”.

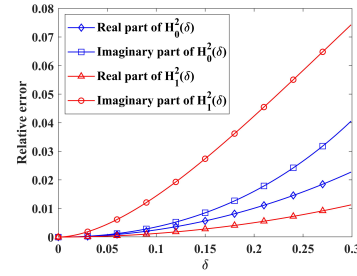


Fig. 4. The relative error of the small variable expansion compared with Hankle function when different δ is used. The reference results come from the Matlab command “besselj(order, δ)” and “bessely(order, δ)”.

We assume that all \mathbf{r}' located on $[\mathbf{r}'_1, \mathbf{r}'_2]$ satisfy the condition of small variable expansion, $|k(\mathbf{r} - \mathbf{r}')| < \delta$. When the observation point is fixed at \mathbf{r} , and corresponding testing function $\mathbf{f}_m(\mathbf{r})$ is used, the analytical results of \mathcal{L} and \mathcal{K} are expressed as (35) and (36). a_1, a_2, a_3, a_4 are constants defined as

$$\begin{aligned} a_1 &= \omega\mu / (4|\mathbf{r}'_1 - \mathbf{r}'_2|), & a_2 &= -1 / (2\pi|\mathbf{r}'_1 - \mathbf{r}'_2|), \\ a_3 &= j(k^2/8|\mathbf{r}'_1 - \mathbf{r}'_2|), & a_4 &= -j(2/\pi) \ln(\gamma k/2), \end{aligned} \quad (37)$$

and $\mathbf{v}_1, \mathbf{v}_2, \mathbf{v}_3, \mathbf{v}_4$ are constant vectors defined as

$$\begin{aligned} \mathbf{v}_1 &= \mathbf{f}_m \cdot \{[\mathbf{n}' \times (\mathbf{r}'_1 - \mathbf{p})] \times \tau'\}, \\ \mathbf{v}_2 &= \mathbf{f}_m \cdot \{[\mathbf{n}' \times (\mathbf{r}'_1 - \mathbf{p})] \times (\mathbf{r} - \mathbf{p})\}, \\ \mathbf{v}_3 &= \mathbf{f}_m \cdot \mathbf{n}', & \mathbf{v}_4 &= \mathbf{f}_m \cdot \vec{\tau} \cdot |(\mathbf{r} - \mathbf{p})|. \end{aligned} \quad (38)$$

In (35) and (36), $I_1 \sim I_8$ are the integrals defined in the Appendix. Here, we use one half of the basis function as a computational example, and the other half can be computed similarly.

If the Galerkin scheme is used to calculate (4) and (5), there are two integral variables. The outer line integration is defined for \mathbf{r} and the inner line integration is for \mathbf{r}' . Considering an arbitrary pair of observation and source segments, we proposed an approach to calculate the nearly singular and singular

$$\mathbf{f}_m(\mathbf{r}) \cdot \mathcal{L}[\mathbf{f}_n(\mathbf{r}')] d\mathbf{r}' = a_1 \mathbf{f}_m(\mathbf{r}) \cdot [(\mathbf{p} - \mathbf{r}'_1) (I_1 + I_6) + a_4 I_2 + I_7] - a_1 \nabla \cdot \mathbf{f}_m(\mathbf{r}) \cdot [a_4 I_1 + I_6] \quad (35)$$

$$\mathbf{f}_m(\mathbf{r}) \cdot \mathcal{K}[\mathbf{n}' \times \mathbf{f}_n(\mathbf{r}')] d\mathbf{r}' = \mathbf{v}_1 (a_3 I_8 + a_2 I_4) + \mathbf{v}_2 (a_3 I_6 + a_2 I_3) + \mathbf{v}_3 (a_3 I_8 + a_2 I_5) + \mathbf{v}_4 (a_3 I_7 + a_2 I_4) \quad (36)$$

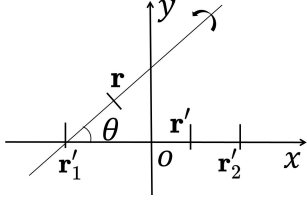


Fig. 5. A source segment with the endpoints $\mathbf{r}'_1(-0.065, 0, 0)$ [m] and $\mathbf{r}'_2(0.065, 0, 0)$ [m] is considered. \mathbf{r} is the observation point, which is 0.02 m away from \mathbf{r}'_1 . θ changes from 0.05π to π .

integration in the proposed SS-SIE formulation as described below.

- 1) For the outer line integration, Gaussian quadrature is used to calculate the integrals for \mathbf{r} . The integration accuracy will increase when more Gaussian points are used [51].
- 2) For the inner integration, an approach combining the analytical integration approach and Gaussian quadrature is used. When a Gaussian point on the observation segment is fixed, the part of source segment, which satisfies $|k(\mathbf{r} - \mathbf{r}')| < \delta$, is analytically calculated by (35) and (36) (shown at the bottom of this page), and the remaining parts are evaluated by the Gaussian quadrature.

The proposed integration approach is applicable not only when the source and observation segments are overlapped, but also for strong nearly singular integrals when the source and observation segments are near to each other.

V. NUMERICAL RESULTS AND DISCUSSION

A numerical example is first carried out to verify the convergence of the proposed integration approach in Section IV. Then, two TE-polarization scattering problems are solved to demonstrate the performance of the proposed SS-SIE formulation.

A personal laptop with Intel i7-7770 3.6 GHz CPU and 48G memory is used for all the experiments in this Section. Our in-house codes, including the proposed SS-SIE formulation and the PMCHWT formulation, are implemented in Matlab, and full vectorization is exploited for both approaches to enhance the performance. Only a single thread is used for a fair comparison. In addition, the Legendre polynomial is used for the general Gaussian quadrature rule to compute the Gaussian points and weights.

A. Validation of the Proposed Integration Approach

An example presented in Fig. 5 is used to verify the efficiency and accuracy of the proposed integration approach. As shown in Fig. (5), $\mathbf{r}'_1(-0.065, 0, 0)$ [m] and $\mathbf{r}'_2(0.065, 0, 0)$ [m] are the endpoints of source segment, and the observation point \mathbf{r} is 0.02 m away from \mathbf{r}'_1 . θ is the angle between $(\mathbf{r}'_1 - \mathbf{r})$ and $(\mathbf{r}'_1 - \mathbf{r}'_2)$. (35) and (36) are used to calculate the integration when $|k(\mathbf{r} - \mathbf{r}')| < \delta$, and the Gaussian quadrature is used for the remaining parts. In the computation, we use $k = 1 \text{ m}^{-1}$ for convenience. We used the proposed integration

approach and the Gaussian quadrature to calculate \mathcal{L} and \mathcal{K} operators. We keep increasing the integration points in the Gaussian quadrature until $|(t_{n+1} - t_n)|/t_{n+1} < 10^{-15}$, where t_n denotes the integration results obtained from the Gaussian quadrature with n integration points. When the results of \mathcal{L} and \mathcal{K} operators reach convergence precision, we count the number of points used for Gaussian quadrature and the relative error between the two approaches, which represents the overall accuracy of the proposed integration approach.

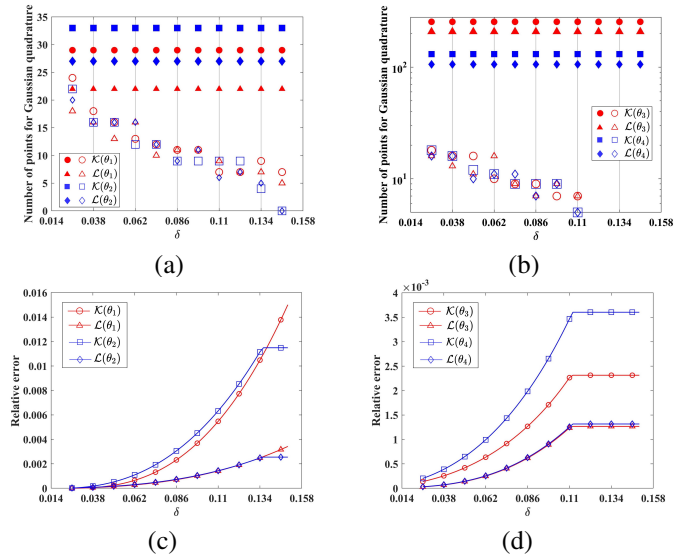


Fig. 6. (a) (b) The color-filled marks are for the fully Gaussian quadrature approach, and the hollow ones are for the proposed integration approach. $\mathcal{K}(\theta)/\mathcal{L}(\theta)$ means that the results are for the \mathcal{K}/\mathcal{L} operator with a certain θ . (c) (d) The corresponding precision when the results reach convergence. $\theta_1 = \pi$, $\theta_2 = 0.5\pi$ in (a) and (c). $\theta_3 = 0.05\pi$, $\theta_4 = 0.1\pi$ in (b) and (d).

From Fig. 6(a) and (b), it can be found that the number of integration points used for Gaussian quadrature increases when δ decreases. Meanwhile, the overall accuracy of the proposed integration approach is higher when δ decreases, as shown in Fig. 6(c) and (d). This is because a small δ can better approximate the Hankel function and its gradient, as shown in Fig. 4. Therefore, a balance between computational efficiency and accuracy is needed. In Fig. 6(b), the number of integration points required for the Gaussian quadrature is large, since θ is very small and strong nearly singular integrals are involved in \mathcal{L} and \mathcal{K} . Therefore, we need an appropriate δ to accurately and efficiently calculate the integration. As shown in Fig. 6, $\delta = 0.1$ is accurate enough for most applications. The proposed integration approach only needs less than ten integration points, which is less than half of integration points with the Gaussian quadrature. It should be noted that the y -axis in Fig. 6(b) is in log scale for better visualization. It can be found that there are no marks in the large δ region of Fig. 6(b), and the curves of Fig. 6(c) and (d) become flat when δ is larger than specific values. This is because the small variable approximation condition is satisfied in the whole source segment, and (35) and (36) are used to calculate the integration without the Gaussian quadrature.

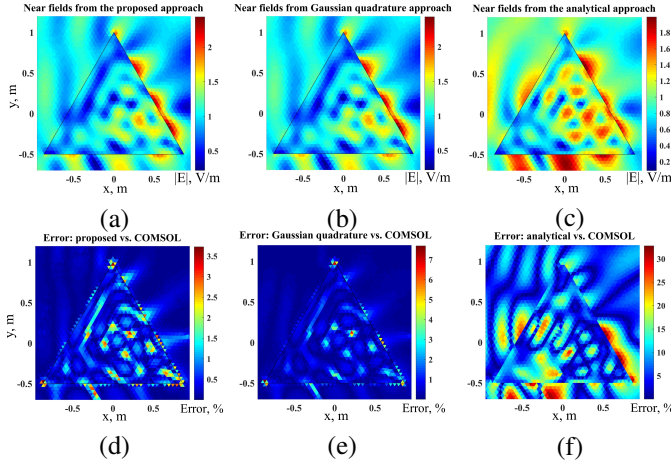


Fig. 7. The near fields from (a) the proposed integration approach, (b) the Gaussian quadrature and (c) the analytical approach. (d) (e) (f) The relative errors compared with the results from COMSOL.

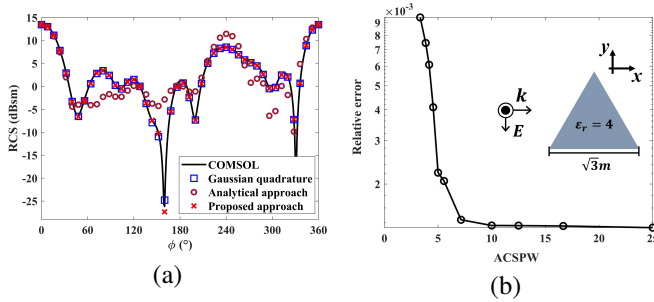


Fig. 8. (a) RCS obtained from the proposed SS-SIE formulation, the analytical approach, the fully Gaussian quadrature approach, and the COMSOL. (b) The relative error compare to the results from COMSOL when different mesh size is used.

B. A Single Penetrable Object

An object whose cross-section is an equilateral triangle is carried out to validate the accuracy and efficiency of the proposed integration approach. The side length of the triangle is $\sqrt{3}$ m, and the relative permittivity inside it is 4. The surrounding medium is air. A TE-polarized plane wave with the frequency of 300 MHz incidents from the x -axis. The averaged length of the segments used to discretize the contour of the triangle is $\lambda/10$, where λ is the wavelength inside the penetrable object. In our comparisons, the proposed SS-SIE formulation incorporated with three integration approaches (namely, the proposed integration approach, the analytical approach [41, Ch.3, pp. 43-44] [42], and the Gaussian quadrature), are used. In the analytical approach, only the self segments are treated to be singular. Then, the Green's function and its gradient are approximated by (33) and (34), and analytical integration is applied. Other integration are calculated through Gaussian quadrature. 14-point and 5-point Gaussian quadrature for the source and observation line integration are used.

The near- and far-fields obtained from the three approaches are shown in Fig. 7 and 8. The reference results are calculated from the COMSOL with fine mesh. The relative error of the proposed SS-SIE formulation is less than 4% compared with the COMSOL, as shown in Fig. 7(d). In addition, it is found that the accuracy of the proposed integration approach is about

twice better than that of the Gaussian quadrature, as shown in Fig. 7(d) and (e). The RCS obtained from the proposed integration approach and the Gaussian quadrature shows excellent agreements with the results from the COMSOL. However, the results from the analytical approach are the worst among the three formulations for both near fields and far fields, as shown in Fig. 7(f) and Fig. 8(a). The reason may be the inconsistency of the accuracy. It can be found from Section V-A that 14 points may not be accurate enough to evaluate the integration, especially when the observation point is very close to the source segment (e.g., at vertices of the triangle). In the analytical approach, the results are accurate when the observation segment is overlapped with the source segment, but are not accurate enough when the observation segment is close to the source segment. However, when the Gaussian quadrature is used, the results are much more accurate than those of the analytical approach. This may be due to the fact that the accuracy of the Gaussian integral is uniform when the observation segment is overlapped or close to the source segment.

In Fig. 8(b), the relative error with respect to averaged count of segments per wavelength (ACSPW) in the free space is shown, and the stability of the proposed integration approach is proved again. The relative error used here is defined as

$$\frac{\sum_i \|\text{RCS}^{\text{cal}}(\phi_i) - \text{RCS}^{\text{ref}}(\phi_i)\|^2}{\sum_i \|\text{RCS}^{\text{ref}}(\phi_i)\|^2}, \quad (39)$$

where $\text{RCS}^{\text{cal}}(\phi_i)$ denotes results calculated from the proposed SS-SIE formulation and $\text{RCS}^{\text{ref}}(\phi_i)$ is the reference results obtained from the COMSOL.

C. An Array with 5×5 Multilayered Coated Dielectric Cylinders

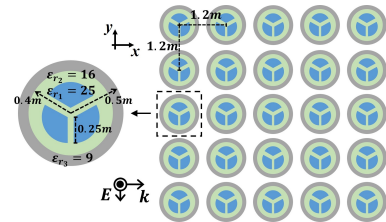


Fig. 9. An array with 5×5 multi-layered coated dielectric cylinders.

In this subsection, an array with 5×5 multilayered coated dielectric cylinder is simulated, as shown in Fig. 9. The innermost cylinder is simulated, as shown in Fig. 9. The innermost sectors are dielectric objects with $r_1 = 0.25$ m and $\epsilon_{r1} = 25$. The second layer is dielectric with $r_2 = 0.4$ m and $\epsilon_{r2} = 16$. The third layer is a dielectric ring with $r_3 = 0.5$ m and $\epsilon_{r3} = 9$. The central distance between two adjacent elements is $d = 1.2$ m, and the background medium is air. The TE-polarized plane wave with $f = 300$ MHz incidents from the x -axis. $\lambda_0/40$ is used to discretize all boundaries, where λ_0 is the free-space wave length.

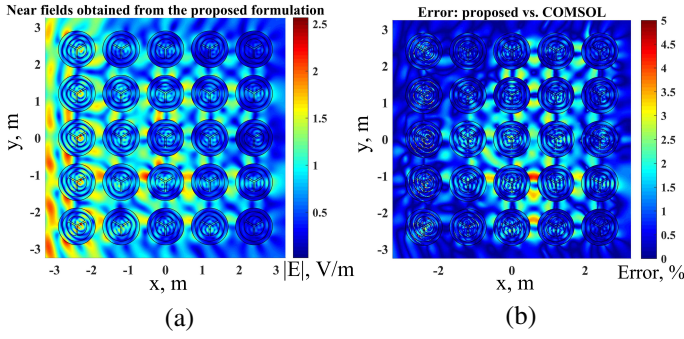


Fig. 10. (a) The near field from the proposed SS-SIE formulation for the array in Fig. 9. (b) The relative error compared with COMSOL.

TABLE I
COMPARISON OF COMPUTATIONAL COST FOR THE PMCHWT FORMULATION AND THE PROPOSED SS-SIE FORMULATION

	PMCHWT	Proposed	Ratio
Overall Time Cost [s]	3,600	1,037	0.29
Time for Matrices Filling [s]	3420	1,039	0.30
Time for \mathbb{Y}_s Generation[s]	—	0.4	—
Time for Equation Solving [s]	176	5.6	0.03
Memory Consumption [MB]	5189	1,331	0.26
Number of Unknowns	20,700	4,000	0.19

TABLE II
COMPARISON OF THE CONDITION NUMBER BETWEEN THE PROPOSED SS-SIE FORMULATION AND THE PMCHWT FORMULATION

Condition Number							
Proposed						PMCHWT	
1st	$\mathbb{L}_{(1,1)}^{(1)}$	17	$\mathbb{L}_{(2,2)}^{(1)}$	17	$\mathbb{L}_{(3,3)}^{(1)}$	17	185,017 (w/o equilibration)
	$\widehat{\mathbb{L}}_{(1,1)}^{(1)}$	11	$\widehat{\mathbb{L}}_{(2,2)}^{(1)}$	11	$\widehat{\mathbb{L}}_{(3,3)}^{(1)}$	11	
2nd	\mathbb{C}_{γ_1}	161	\mathbb{V}_{γ_4}	51	$\widehat{\mathbb{L}}_{(4,4)}^{(2)}$	101	66,101 (diagonal)
3rd	\mathbb{C}_{γ_2}	551	\mathbb{V}_{γ_5}	131	$\widehat{\mathbb{L}}_{(5,5)}^{(3)}$	88	1,924 (extended diagonal)
Solving	$\mathbb{U} - \widehat{\mathbb{L}}\mathbb{Y}_s$			1,257 (w/o equilibration)			

The near fields of the array are shown in Fig. 10(a), and the relative error compared with the COMSOL is presented in Fig. 10(b). It can be found that the relative error is less than 5%. The RCS is computed by the proposed SS-SIE formulation, the PMCHWT formulation, and the COMSOL, as shown in Fig. 11(a). The results obtained from the proposed SS-SIE formulation are in excellent agreement with the results from the PMCHWT formulation and the COMSOL.

Table I shows the computational cost of the PMCHWT formulation and the proposed SS-SIE formulation. PMCHWT formulation has 20,700 unknowns while the proposed SS-SIE formulation only requires 4,000. This smaller number is due to the fact that the only electric current density residing on the outermost boundary is required with the proposed SS-SIE formulation. For the memory consumption, 5,189 MB

memory is used in the PMCHWT formulation, only 1,331 MB memory, 26% of the PMCHWT formulation, is used with the proposed SS-SIE formulation. The CPU time to fill the coefficient matrix is 3,420 s with the PMCHWT formulation and 1,039 s with the proposed SS-SIE formulation. Therefore, the CPU time is reduced by 71%. Since there is only one type of scatters in this array, the DSAO is needed to be calculated once, which uses 0.4 s. Therefore, the saving in terms of memory and CPU time is significant with the proposed formulation. Although there are 13 matrices to be inverted with the proposed formulation, all the matrices have smaller dimensions with the largest dimension being 4,000.

To construct the surface equivalent current density on the outermost boundary, the surface equivalence theorem is applied three times. As shown in Table II, the matrix condition number of the PMCHWT formulation is 185,017. However, the condition number of the final matrix of the proposed approach is only 1,257. For the PMCHWT formulation, all geometric details are in the final large matrix, but they are implicitly incorporated into several small matrices with the proposed SS-SIE formulation. Therefore, the condition number of the final system is smaller with the proposed SS-SIE formulation.

There are several methods to decrease the condition number in SIE, like matrix equilibration [52]. We applied diagonal scaling and extended scaling to balance the source and functions in both the PMCHWT formulation and the proposed formulation. As shown in Table I, the condition number decreases significantly in PMCHWT formulation. However, the matrix equilibration has little effect on the proposed formulation. This may be due to the fact that only a single electric current and EFIE are applied in the proposed formulation.

In addition, the same structure with high permittivity, which is $\varepsilon_{r_1} = 125$ for the innermost objects, $\varepsilon_{r_2} = 75$ for the second layer, and $\varepsilon_{r_3} = 25$ for the third layer, is modeled to validate the robustness of the proposed SS-SIE formulation. Fig. 11(b) shows the RCS with the the PMCHWT formulation, the proposed formulation, and the COMSOL. They show excellent agreement with each other. Therefore, the proposed SS-SIE formulation can model the structures with high permittivity.

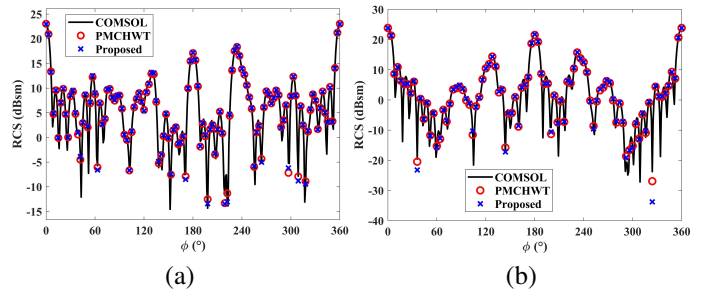


Fig. 11. RCS obtained from the COMSOL, the PMCHWT formulation, and the proposed SS-SIE formulation in case of (a) low permittivity and (b) high permittivity.

D. Discussion

Assuming there are p layers with $N_1, N_2, N_3, \dots, N_p$ segments on each boundary, and $N = N_1 + N_2 + \dots + N_p$

segments in all. For the matrix filling, the computational complexity of the proposed SS-SIE formulation is more than $O(N_1^2) + O(N_2^2) + \dots + O(N_p^2)$ and less than $O(N^2)$. For the matrix equation solving, the computational complexity is $O(N_1^3) + O(N_2^3) + \dots + O(N_{i-1}^3) + O(N_i^3)$. Therefore, the proposed formulation has a lesser computational complexity than that of the PMCHWT formulation in most occasions ($O(N^2)$ for the matrix filling and $O(N^3)$ for matrix solving).

However, the proposed SS-SIE formulation suffers from efficiency issue for large structures since the construction of the DSAO requires dense matrix inversion. The overhead cannot be ignored for those large structures. There are basically two ways to overcome this issue. One way is to use efficient direct algorithms, such as H-Matrix [53], HSS solver [54], and so on. The other efficient way is to partition the large objects into small ones. The DSAO is constructed for those small objects, and the efficiency is improved.

In addition, the proposed formulation may have problems at the resonant frequencies since only the EFIE formulation is used to solve the scattering problems. At the resonance, wrong current and large condition number may be obtained due to mode degeneration. In [17], a differential surface admittance operator is defined and combined integral field equations are used to avoid resonance.

VI. CONCLUSION

The surface equivalence theorem states that a closed surface with the appropriate surface equivalent current sources can generate external fields precisely the same as those in the original problems. In this paper, we thoroughly explore this possibility with the method of moments implementations. A novel vector SS-SIE is proposed to solve TE scattering problems for objects embedded in cylindrical multilayers. The proposed method employs the full vector electromagnetic formulations and extends our previous work in [47] which only works for the scalar TM-polarized electromagnetic problems.

The proposed SS-SIE formulation only needs a single electric current density on the outermost boundary. It is derived by recursively applying the surface equivalence theorem on each boundary from inner to exterior regions. Compared with the PMCHWT formulation, the proposed SS-SIE formulation can improve computational efficiency in terms of the number of unknowns, memory consumption, CPU time, and the system's conditioning number. In addition, to accurately handle the nearly singular and singular integrals in the proposed SS-SIE formulation, an integration approach is proposed. Numerical results validate the efficiency and convergence property of the proposed integration approach and SS-SIE formulation.

Extension of the current work into the three-dimensional case and fast direct solver to accelerate construction \mathbb{Y}_n is in progress. We will report more results on this topic in the future.

APPENDIX

According to the definitions in Section IV, the following eight identities [39] [55, Ch. 5] are used.

$$I_1 = \int_l \ln |\mathbf{r} - \mathbf{r}'| d\mathbf{r}'$$

$$= l_2 \ln |\mathbf{r} - \mathbf{r}_2| - l_1 \ln |\mathbf{r} - \mathbf{r}_1| + |\mathbf{r} - \mathbf{p}|.$$

$$\left(\tan^{-1} \frac{l_2}{|\mathbf{r} - \mathbf{p}|} - \tan^{-1} \frac{l_1}{|\mathbf{r} - \mathbf{p}|} \right) - (l_2 - l_1), \quad (40)$$

$$I_2 = \int_l \vec{l} \cdot \ln |\mathbf{r} - \mathbf{r}'| d\mathbf{r}' = \frac{\vec{r}}{2} \cdot \left\{ -\frac{1}{2} [(l_2)^2 - (l_1)^2] + |\mathbf{r} - \mathbf{r}_2|^2 \ln |\mathbf{r} - \mathbf{r}_2| - |\mathbf{r} - \mathbf{r}_1|^2 \ln |\mathbf{r} - \mathbf{r}_1| \right\}, \quad (41)$$

$$I_3 = \int_l \frac{1}{|\mathbf{r} - \mathbf{r}'|^2} d\mathbf{r}' \quad (42)$$

$$= \frac{1}{|\mathbf{r} - \mathbf{p}|} \left(\tan^{-1} \frac{l_2}{|\mathbf{r} - \mathbf{p}|} - \tan^{-1} \frac{l_1}{|\mathbf{r} - \mathbf{p}|} \right), \quad (43)$$

$$I_4 = \int_{l_i} \frac{|\vec{l}|}{|\mathbf{r} - \mathbf{r}'|^2} d\mathbf{r}' = (\ln |\mathbf{r} - \mathbf{r}_2| - \ln |\mathbf{r} - \mathbf{r}_1|), \quad (44)$$

$$I_5 = \int_l \frac{\vec{l} \cdot \vec{l}}{|\mathbf{r} - \mathbf{r}'|^2} d\mathbf{r}' = (l_2 - l_1) - |\mathbf{r} - \mathbf{p}|^2 \cdot I_3, \quad (45)$$

$$I_6 = \int_l 1 d\mathbf{r}' = l_2 - l_1, \quad (46)$$

$$I_7 = \int_l |\vec{l}| d\mathbf{r}' = \frac{1}{2} [(l_2)^2 - (l_1)^2], \quad (47)$$

$$I_8 = \int_l \vec{l} \cdot \vec{l} d\mathbf{r}' = \frac{1}{3} [(l_2)^3 - (l_1)^3]. \quad (48)$$

Based on the above eight integrals, we can accurately calculate the nearly singular and singular integrals in (4) and (5) in the proposed SS-SIE formulation.

REFERENCES

- [1] P. Mojabbi and J. LoVetri, "Comparison of TE and TM inversions in the framework of the Gauss-Newton method," *IEEE Trans. Antennas Propag.*, vol. 58, no. 4, pp. 1336-1348, Apr. 2010.
- [2] W. C. Chew, J. M. Jin, E. Michielssen and J. Song, Eds, *Fast and Efficient Algorithms in Computational Electromagnetics*, Norwood, MA: Artech House, 2001.
- [3] K. Sertel, "Multilevel fast multipole method for modeling permeable structures using conformal finite elements," Ph.D. dissertation, Dept. Elect. Comput. Eng., Univ. Michigan at Ann Arbor, Ann Arbor, MI, 2003.
- [4] A. J. Poggio and E. K. Miller, "Integral equation solutions of three-dimensional scattering problems," in *Computer Techniques for Electromagnetics*. R. Mittra, Ed. Oxford, UK: Pergamon, 1973.
- [5] P. Ylä-Oijala, M. Taskinen, and S. Järvenpää, "Surface integral equation formulations for solving electromagnetic scattering problems with iterative methods," *Radio Sci.*, vol. 40, no. 6, pp. 1-19, Dec. 2005.
- [6] C. Müller, *Foundations of the Mathematical Theory of Electromagnetic Waves*. New York: Springer-Verlag, 1969.
- [7] J. Hu, R. Zhao, Y. Zhang, M. Jiang and Z. Nie, "Fast solving EM scattering from penetrable objects with non-conformal multiple-traces PMCHWT equations," in *IEEE Int. Conf. Ubiquitous Wirel. Broadband (ICUWB)*, Nanjing, Dec. 2016.
- [8] A. Menshov and V. Okhmatovski, "New single-source surface integral equations for scattering on penetrable cylinders and current flow modeling in 2-D conductors," *IEEE Trans. Microw. Theory Techn.*, vol. 61, no. 1, pp. 341-350, Jan. 2013.
- [9] F. S. H. Lori, A. Menshov, and V. Okhmatovski, "New vector single-source surface integral equation for scattering problems on dielectric objects in 2-D," *IEEE Trans. Antennas Propag.*, vol. 65, pp. 3794-3799, Jul. 2017.
- [10] F. S. H. Lori, M. S. Hosen, and V. Okhmatovski, "Higher order method of moments solution of the new vector single-source surface integral equation for 2D TE scattering by dielectric objects," in *IEEE MTT-S Int. Conf. Numer. Electromagn. Multiphysics Model. Optim. RF, Microw., Terahertz Appl. (NEMO)*, Seville, 2017, pp. 161-163.

- [11] Z. G. Qian, W. C. Chew, and R. Suaya, "Generalized impedance boundary condition for conductor modeling in surface integral equation," *IEEE Trans. Microw. Theory Techn.*, vol. 55, no. 11, pp. 2354-2364, Nov. 2007.
- [12] D. De Zutter and L. Knockaert, "Skin effect modeling based on a differential surface admittance operator," *IEEE Trans. Microw. Theory Techn.*, vol. 53, no. 8, pp. 2526-2538, Aug. 2005.
- [13] U. R. Patel and P. Triverio, "Skin effect modeling in conductors of arbitrary shape through a surface admittance operator and the contour integral method," *IEEE Trans. Microw. Theory Techn.*, vol. 64, no. 9, pp. 2708-2717, Sep. 2016.
- [14] U. R. Patel, B. Gustavsen, and P. Triverio, "Proximity-aware calculation of cable series impedance for systems of solid and hollow conductors," *IEEE Trans. Power Del.*, vol. 29, no. 5, pp. 2101-2109, Oct. 2014.
- [15] U. R. Patel and P. Triverio, "MoM-SO: a complete method for computing the impedance of cable systems including skin, proximity, and ground return effects," *IEEE Trans. Power Del.*, vol. 30, no. 5, pp. 2110-2118, Oct. 2015.
- [16] M. Huynen, D. De Zutter, and D. Vande Ginste, "A fully 3-D BIE evaluation of the resistance and inductance of on-board and on-chip interconnects," in *IEEE 22nd Work. Signal Power Integr.*, Brest, Jul. 2018.
- [17] U. R. Patel, P. Triverio, and S. V. Hum, "A novel single-source surface integral method to compute scattering from dielectric objects," *IEEE Antennas Wirel. Propag. Lett.*, vol. 16, pp. 1715-1718, Feb. 2017.
- [18] U. R. Patel, P. Triverio, and S. V. Hum, "A macromodeling approach to efficiently compute scattering from large arrays of complex scatterers," *IEEE Trans. Antennas Propag.*, vol. 66, no. 11, pp. 6158-6169, Nov. 2018.
- [19] M. Huynen, M. Gossye, D. De Zutter, and D. Vande Ginste, "A 3-D differential surface admittance operator for lossy dipole antenna analysis," *IEEE Antennas Wirel. Propag. Lett.*, vol. 16, pp. 1052-1055, Oct. 2017.
- [20] M. Huynen, D. De Zutter, and D. Vande Ginste, "Broadband 3-D boundary integral equation characterization of composite conductors," in *IEEE Conf. Electr. Perform. Electron. Packag. Syst.(EPEPS)*, Montreal, Apr. 2020.
- [21] M. Huynen, K. Y. Kapsuz, X. Sun, G. V. D. Plas, E. Beyne, D. De Zutter, and D. Vande Ginste, "Entire domain basis function expansion of the differential surface admittance for efficient broadband characterization of lossy interconnects," *IEEE Trans. Microw. Theory Techn.*, vol. 68, no. 4, pp. 1217-1233, Apr. 2020.
- [22] Y. Shi, C. H. Liang, "An efficient single-source integral equation solution to EM scattering from a coated conductor," *IEEE Antennas Wirel. Propag. Lett.*, vol. 14, pp. 547-550, Nov. 2014.
- [23] F. S. H. Lori, M. S. Hosen, and V. Okhmatovski, "Higher order method of moments solution of the new vector single-source surface integral equation for 2D TE scattering by dielectric objects," in *IEEE MTT-S Int. Conf. Numer. Electromagn. Multiphysics Model. Optim. RF, Microw., Terahertz Appl. (NEMO)*, Seville, Jul. 2017.
- [24] F. S. H. Lori, A. Moshov, R. Gholami, J. Mojolagbe, and V. Okhmatovski, "Novel single-source surface integral equation for scattering problems by 3-D dielectric objects," *IEEE Trans. Antennas Propag.*, vol. 66, no. 2, pp. 797-807, Feb. 2018.
- [25] D. R. Swatek and I. R. Ciric, "Single source integral equation for wave scattering by multiply-connected dielectric cylinders," *IEEE Trans. Magn.*, vol. 32, no. 3, pp. 878-881, May. 1996.
- [26] M. K. Li and W. C. Chew, "Wave-field interaction with complex structures using equivalence principle algorithm," *IEEE Trans. Antennas Propag.*, vol. 55, no. 1, pp. 130-138, Jan. 2007.
- [27] M. K. Li and W. C. Chew, "Multiscale simulation of complex structures using equivalence principle algorithm with high-order field point sampling scheme," *IEEE Trans. Antennas Propag.*, vol. 56, no. 8, pp. 2389-2397, Aug. 2008.
- [28] F. G. Hu and J. M. Song, "Integral equation analysis of scattering from multilayered periodic array using equivalence principle and connection scheme," *IEEE Trans. Antennas Propag.*, vol. 58, no. 3, pp. 848-856, Mar. 2010.
- [29] C. Balanis, *Antenna Theory: Analysis and Design*. 3rd ed. Wiley, 2005.
- [30] K. Chen and J. M. Song, "Singularity subtraction for nearly singular integrals on curvilinear triangular elements," *IEEE Antennas Wirel. Propag. Lett.*, vol. 14, pp. 1435-1438, Mar. 2015.
- [31] S. Jarvenpaa, M. Taskinen and P. Yla-Oijala, "Singularity subtraction technique for high-order polynomial vector basis functions on planar triangles," *IEEE Trans. Antennas Propag.*, vol. 54, no. 1, pp. 42-49, Jan. 2006.
- [32] E. Simsek, Q. H. Liu and B. J. Wei, "Singularity subtraction for evaluation of Green's functions for multilayer media," *IEEE Trans. Microw. Theory Techn.*, vol. 54, no. 1, pp. 216-225, Jan. 2006.
- [33] R. D. Graglia and G. Lombardi, "Machine precision evaluation of singular and nearly singular potential integrals by use of gauss quadrature formulas for rational functions," *IEEE Trans. Antennas Propag.*, vol. 56, no. 4, pp. 981-998, Apr. 2008.
- [34] M. A. Khayat and D. R. Wilton, "Numerical evaluation of singular and near-singular potential integrals," *IEEE Trans. Antennas Propag.*, vol. 53, no. 10, pp. 3180-3190, Oct. 2005.
- [35] A. G. Polimeridis, F. Vipiana, J. R. Mosig, and D. R. Wilton, "DI-RECTFN: Fully numerical algorithms for high precision computation of singular integrals in Galerkin SIE methods," *IEEE Trans. Antennas Propag.*, vol. 61, no. 6, pp. 3112-3122, Jun. 2013.
- [36] A. J. Krneta and B. M. Kolundzija, "Evaluation of potential and impedance integrals in analysis of axially symmetric metallic structures to prescribed accuracy up to machine precision," *IEEE Trans. Antennas Propag.*, vol. 65, no. 5, pp. 2526-2539, May 2017.
- [37] A. J. Krneta and B. M. Kolundzija, "Using ultra-high expansion orders of max-ortho basis functions for analysis of axially symmetric metallic antennas," *IEEE Trans. Antennas Propag.*, vol. 66, no. 7, pp. 3696-3699, Jul. 2018.
- [38] J. G. Perovic, D. I. Olcan, B. M. Kolundzija and A. R. Djordjevic, "A singularity cancelation transformation for entire-domain analysis of 2-D structures with high-precision integration," *IEEE Trans. Antennas Propag.*, vol. 67, no. 4, pp. 2522-2533, Apr. 2019.
- [39] D. Wilton, S. Rao, A. Glisson, D. Schaubert, O. Al-Bundak and C. Butler, "Potential integrals for uniform and linear source distribution on polygonal and polyhedral domains," *IEEE Trans. Antennas Propag.*, vol. 32, no. 3, pp. 276-281, Mar. 1984.
- [40] Y. F. Jing and T. Z. Huang, "A novel integration method for weak singularity arising in two-dimensional scattering problems," *IEEE Trans. Antennas Propag.*, vol. 58, no. 8, pp. 2725-2731, Aug. 2010.
- [41] R. F. Harrington, *Field Computation by Moment Methods*. New York: Macmillan, 1968.
- [42] Y. Liu, H. Z. Yang, "A hierarchical butterfly LU preconditioner for two-dimensional electromagnetic scattering problems involving open surfaces," *J. Comput. Phys.*, vol. 401, Jan. 2020.
- [43] W. Gibson, *The Method of Moments in Electromagnetics*. CRC press, 2015.
- [44] M. A. Jensen and J. D. Freeze, "A recursive Green's function method for boundary integral analysis of inhomogeneous domains," *IEEE Trans. Antennas Propag.*, vol. 46, no. 12, pp. 1810-1816, Dec. 1998.
- [45] D. R. Swatek and I. R. Ciric, "A recursive single-source surface integral equation analysis for wave scattering by heterogeneous dielectric bodies," *IEEE Trans. Antennas Propag.*, vol. 48, no. 8, pp. 1175-1185, Aug. 2000.
- [46] X. C. Zhou, Z. K. Zhu, S. C. Yang, and D. L. Su, "A novel single source surface integral equation for electromagnetic analysis by multilayer embedded objects," in *Int. Appl. Comput. Electromagn. Soc. Symp.-China (ACES)*, Nanjing, 2019.
- [47] X. C. Zhou, Z. K. Zhu, and S. C. Yang, "Towards a unified approach to electromagnetic analysis of objects embedded in multilayers," *J. Comput. Phys.*, vol. 427, Feb. 2021.
- [48] Z. K. Zhu, X. C. Zhou, J. Wang and S. C. Yang, "Single-source SIE for TE electromagnetic analysis of penetrable objects," in *IEEE Int. Symp. Antennas Propag. USNC-URSI Radio Sci. Meet. (APSURSI)*, Montreal, Feb. 2021.
- [49] G. W. Hanson, A. B. Yakovlev, *Operator Theory for Electromagnetics*. Springer, 2002.
- [50] Ö. Ergül, L. Gürel, "The use of curl-conforming basis functions for the magnetic-field integral equation," *IEEE Trans. Antennas Propag.*, vol. 54, no. 7, pp. 1917-1926, Jul. 2006.
- [51] J. Ma, V. Rokhlin and S. Wandzura, "Generalized Gaussian quadrature rules for systems of arbitrary functions," *SIAM J. Numer. Anal.*, vol. 33, pp. 971-996, Jun. 1996.
- [52] B. M. Kolundzija and M. M. Kostic, "Matrix equilibration in method of momentsolutions of surface integral equations," *Radio Sci.*, vol. 49, pp. 1265-1276, Dec. 2014.
- [53] W. W. Chai and D. Jiao, "Fast \mathcal{H} -matrix-based direct integral equation solver with reduced computational cost for large-scale interconnect extraction," *IEEE Trans. Compon. Packag. Manuf. Technol.*, vol. 3, no. 2, pp. 289-298, Feb. 2013.
- [54] S. Chandrasekaran, P. Dewilde, M. Gu, W. Lyons and T. Pals, "A fast solver for HSS representations via sparse matrices," *SIAM J. Matrix Anal. Appl.*, vol. 29, pp. 67-81, Dec. 2006.
- [55] J. Stewart, *Calculus*. Brooks Cole, 2007.